1971, *Phys. Earth Planet. Interiors* **4**, 289–300. North-Holland Publishing Company, Amsterdam

SEISMOLOGICAL EVIDENCE FOR A LITHOSPHERIC NORMAL FAULTING – THE SANRIKU EARTHQUAKE OF 1933

HIROO KANAMORI

Earthquake Research Institute, University of Tokyo, Tokyo, Japan

Received 10 September 1970

The focal process of the Sanriku earthquake of March 2, 1933, is discussed in relation to the bending mechanism of the lithosphere. On the basis of the *P* times obtained at more than 200 stations, it is confirmed that the hypocenter of this earthquake is within the lithosphere beneath the Japan trench. The *P* wave fault plane solution, the amplitude of long-period (100 s) Love and Rayleigh waves and two near-field observations suggest, almost definitely, that the Sanriku earthquake represents a predominantly normal faulting on a plane dipping 45° towards N 90° W. A fault size of 185×100 km^2, in agreement with the size of the aftershock area, is required to yield a slip dislocation of 3.3 m, a value consistent with the tsunami data. This result suggests that the fracture took place over the entire thickness of the lithosphere, thereby precluding the possibility that the Sanriku earthquake merely represents a surface tensile crack due to the bending of the lithosphere. This large scale lithospheric faulting is presumably due to a gravitational pull exerted by the cold sinking lithosphere. The fracture probably took place on an old fault plane which had once fractured and healed up. The existence of this fracture zone which decouples, to some extent, the oceanic lithosphere from the sinking lithosphere accounts for the sharp bend of the lithosphere beneath oceanic trenches and also the abrupt disappearance of seismic activity across oceanic trenches. The sharp bend of the lithosphere is therefore a result, not the cause, of great earthquakes beneath oceanic trenches.

1. Introduction

In the hypothesis of the sea-floor spreading and plate tectonics, the formation, displacement and destruction of the oceanic lithosphere play a fundamental role in explaining various tectonic phenomena such as earthquakes, volcanic activities and heat flow anomalies. At island arcs, in particular, the spatial distribution of shallow, intermediate and deep earthquakes, heat flow distributions and orogenic processes are often discussed in relation to the sinking lithosphere, the Benioff zone. In these discussions, however, it is usually assumed that the lithosphere bends sharply at oceanic trenches and thrusts beneath continents by some "built-in" mechanism. How and why the lithosphere bends sharply and sinks at island arcs are not clearly understood.

The most reliable and quantitative data concerning the deformation of the lithosphere can be obtained by means of detailed seismological analyses of great earthquakes at island arcs. The great earthquakes certainly represent the major tectonic processes; small earthquakes, though numerous, do not primarily contribute to the overall movement of the lithosphere.

This paper discusses, on the basis of seismological data, a possible mode of deformation of the lithosphere at the time of the Sanriku (sometimes called Sanriku-Oki) earthquake of March 2, 1933, to which the largest magnitude ever reported, 8.9, was assigned by RICHTER (1958) (see also GUTENBERG, 1956a). This earthquake is unique among other great earthquakes at island arcs in that its epicenter is very close to the Japan trench; the epicenters of other great earthquakes are much closer to the coast or are even on land. We will first examine the accuracy of the hypocenter location and then determine, on the basis of both near- and far-field displacements, the nature of the faulting. Old seismological data will be analyzed with updated techniques.

2. Hypocenter

The hypocenter of the Sanriku earthquake was redetermined by using the *P* times as listed in the International Seismological Summary (ISS) for the year 1933 and the Seismological Bulletin of the Central Meteorological Observatory of Japan for the year 1933. The Jeffreys–Bullen travel time table was used. We made the relocation for two cases: (1) all the

stations with distance $\Delta \leqq 90°$ except those whose $O-C$ residual (observed minus computed P time) exceeds 30 s were used; (2) stations with $\Delta \leqq 90°$ were used but the $O-C$ threshold was set at 10 s. The number of stations used was 201 in the former case and 186 in the latter. In each case, the depth was restrained at 0, 10, 20, 30, 40, 60, 80 and 100 km and the root-mean-square (RMS) of the $O-C$ residuals was calculated. In both cases, the RMS of $O-C$ was found to increase sharply as the depth increased, favouring a shallow focal depth, probably shallower than 30 km (see fig. 1). In the following discussions, we will place the hypocenter at a depth of 10 km.

Fig. 2 shows the epicenters determined for the two cases together with the epicenters previously determined by MATUZAWA (1935), GUTENBERG and RICHTER (1954) and ISS. The trench axis is also shown for reference. Although the quality of the data obtained in the 1930's may not be very high, we believe that the epicenter determined on the basis of a large number of stations with a good azimuthal coverage as shown in fig. 1 cannot be wrong by more than 20 km. We conclude that the initial break of the Sanriku earthquake occurred within the lithosphere beneath the Japan trench. In the following, we will use the hypocenter parameters determined for the second case: origin time $17^h\ 30^m\ 56^s$; latitude 39.2° N; longitude 144.5° E; depth 10 km.

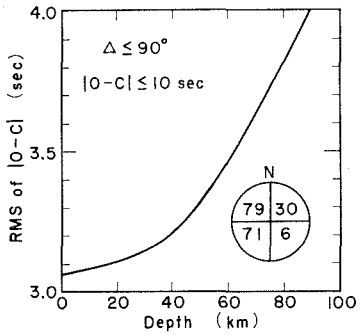

Fig. 1. Root-mean-square (RMS) of $O-C$ residuals as a function of depth. The total number of stations in the NE, SE, SW and NW quadrants is shown in the insert.

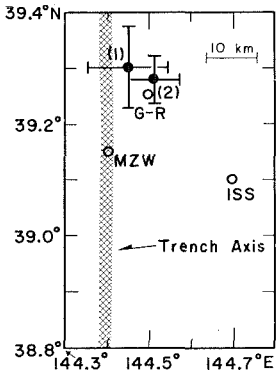

Fig. 2. Epicenters determined for the two cases (1) and (2) (see text). G–R, MZW and ISS are the epicenters determined by GUTENBERG and RICHTER (1954), MATUZAWA (1935) and the International Seismological Summary (1933), respectively. The trench axis is shown for reference.

3. Body-wave fault plane solution

MATUZAWA (1942) determined the direction of the initial motion of P waves on seismograms collected from nearly all the stations in the world. The initial onset of this earthquake is exceptionally sharp (fig. 3) so that the direction of the initial motion can be determined unambiguously. We supplemented Matuzawa's data by Japanese data reported in the Seismological Bulletin of the Central Meteorological Observatory. The results were plotted on the Wulff grid as shown in fig. 4. The lower half of the focal sphere was projected.

In the fault model of earthquakes, the compression and the dilatation fields define two nodal planes. One nodal plane can be determined fairly well as shown in fig. 4. This nodal plane has a dip direction of N 90° W and a dip angle of 45°, and represents a normal faulting. The other nodal plane cannot be determined uniquely because of the unfavourable distribution of stations. A possible range may be set as shown by two nodal planes 1 and 2 in fig. 4. Any nodal plane intermediate between these two can explain the distribution of the observed compressions and dilatations. Despite this uncertainty in the second nodal plane, an important conclusion is that the faulting is, unlike other great earthquakes at island arcs, definitely normal.

An independent determination of the fault planes was made by using S wave polarization angles determined at 9 stations (see fig. 4). HIRASAWA's (1966) method was used. The two nodal planes thus obtained are remarkably consistent with the P wave data as shown in fig. 4 by dash–dot curves. This solution represents an almost pure dip–slip fault with a dip angle of 45°. In view of the uncertainty involved in the deter-

mination of the polarization angles, we will employ, in the following analyses, a pure dip–slip fault with a dip angle of 45°.

Predominance of normal faulting among shallow earthquakes beneath the Aleutian trench was first noted by STAUDER (1968a, b) and discussed in relation to the flexure of the lithosphere. Stauder concluded that these earthquakes are caused by a surface tensile crack upon bending of the lithosphere beneath the Aleutian trench. It should be noted that the Sanriku earthquake is much larger than those studied by Stauder; the magnitude of the earthquakes studied by

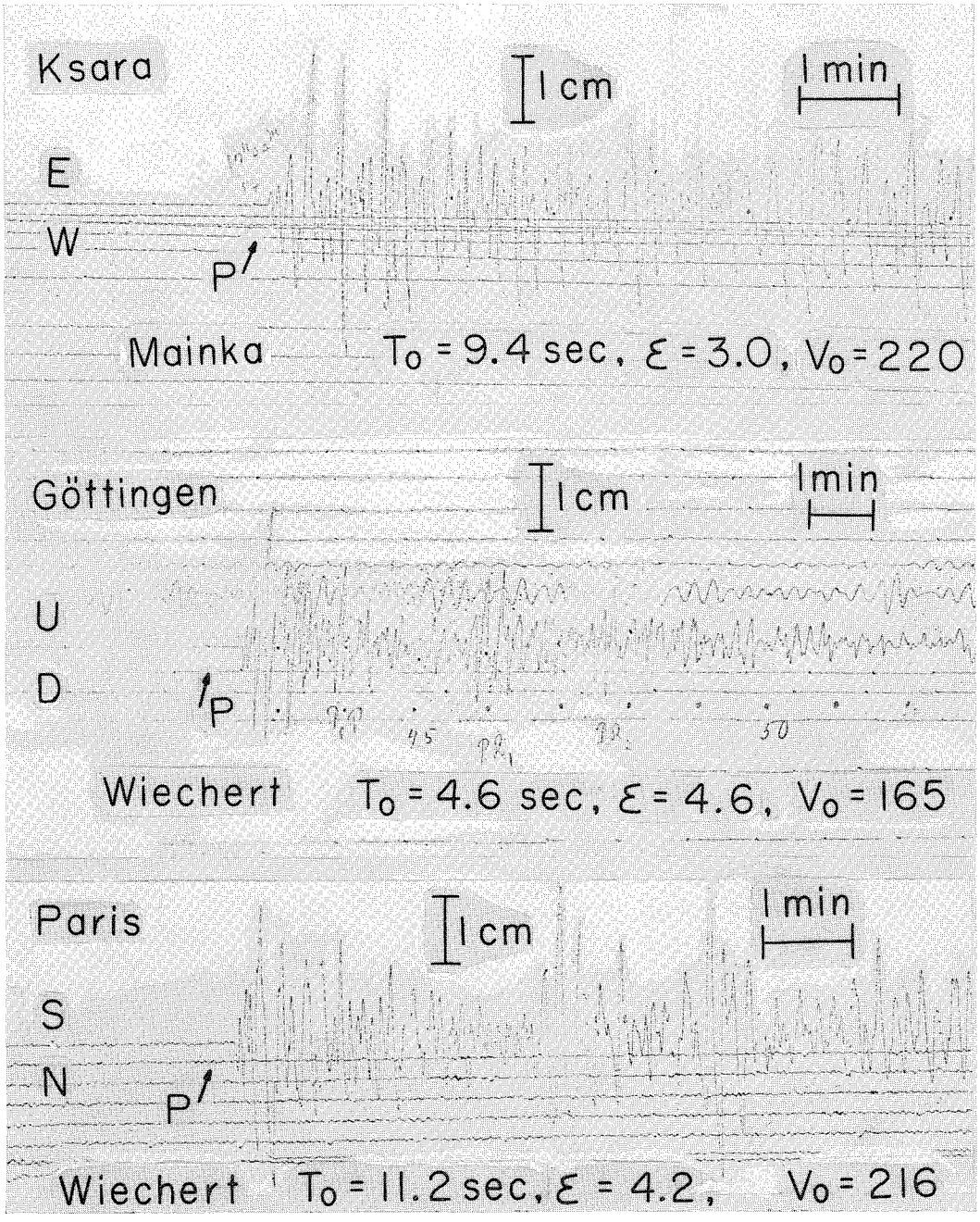

Fig. 3. Examples of seismograms showing P waves of the Sanriku earthquake. T_0 is the pendulum period, ε the damping ratio and V_0 the magnification.

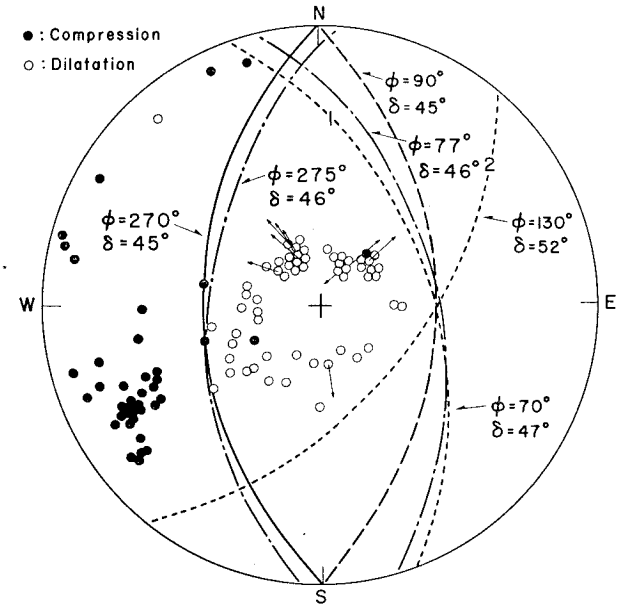

Fig. 4. Stereographic projection of the lower half of the focal sphere on the Wulff grid. ϕ is the dip direction measured clockwise from the north and δ is the dip angle. P wave first motion data (open and closed circles) and the polarization angles of S waves (arrows) are shown. The dash–dot curves show the solution determined by S wave data.

Stauder ranges from 6 to 7. We shall see later that a surface tensile crack alone cannot cause such a great earthquake as the Sanriku earthquake. A process of much larger scale, such as a fracture over the entire thickness of the lithosphere, has to be invoked.

4. Long-period surface waves

AKI (1966) showed that the amplitude of long-period surface waves can be used to determine the slip dislocation on a fault plane. In principle, both the lobe pattern and the amplitude of surface waves can be used to determine the geometry and the slip dislocation. For the Sanriku earthquake, however, the azimuthal coverage of the stations is not good enough to enable one to determine the lobe pattern of the radiation. We therefore fixed the force geometry as determined by the P wave first motions (45° dip slip), calculated theoretical amplitude spectral densities of surface waves for this force system and compared them with the observed spectral densities in order to determine the slip dislocation. We used long-period (about 100 s) surface waves recorded by such classic seismographs as Wiechert, Mainka, etc. Long-period waves from such classic seismograms were successfully used by BRUNE and KING (1967) and BRUNE and ENGEN (1969) to define 100 s magnitude and to estimate seismic moment. Figs. 5(a,b) show several surface wave trains generated by the Sanriku earthquake. These records evidently contain long-period energies up to about 100 s.

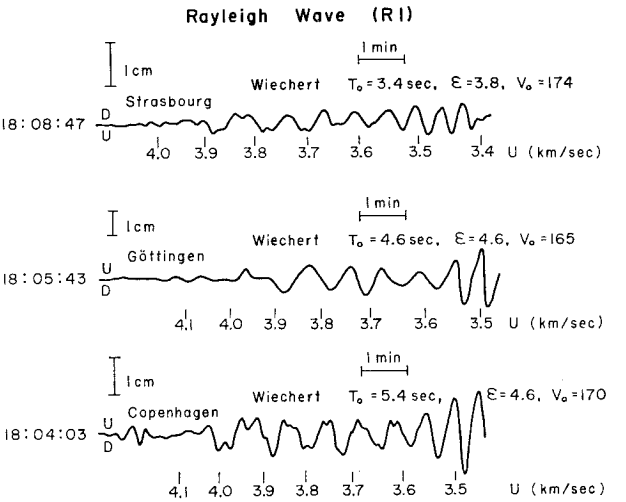

Fig. 5(a). Rayleigh waves observed at Strasbourg, Göttingen and Copenhagen. The times on the left refer to the beginning of the trace; T_0 is the pendulum period, ε the damping ratio and V_0 the magnification. The group velocity scale is given.

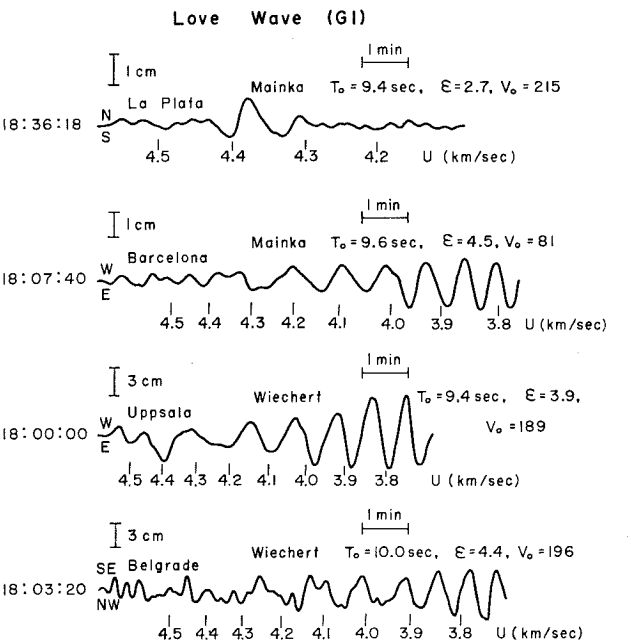

Fig. 5(b). Love waves observed at La Plata, Barcelona, Uppsala and Belgrade. For explanations, see caption of fig. 5a.

We estimated the amplitude spectral density $|A(f)|$ of a seismogram $a(t)$, taken from the original record through group velocity windows appropriate for Love and Rayleigh waves, by

$$|A(f)| = \left| \int_{-\infty}^{+\infty} a(t) \exp(2\pi i f t)\, dt \right|, \qquad (1)$$

where f is the frequency and t is the time. The inverse transform is

$$a(t) = 2 \int_0^{\infty} |A(f)| \cos[2\pi f t + \eta(f)]\, df, \qquad (2)$$

where $\eta(f)$ is the phase delay. The original seismograms at the stations listed in table 1 were digitized at an interval of about 2 s, and the curvature of the stylus motion was corrected. The spectral density was estimated at a period of 100 s by taking the average over a range from 80 to 120 s. Then corrections were made for the seismograph magnification, geometrical ray spreading and attenuation, i.e.

$$|A_0(f)| = |A(f)| \sqrt{\sin\Delta}\, \frac{1}{v} \exp\left[\frac{\pi f \Delta}{QU}\right], \qquad (3)$$

where $|A_0(f)|$ is the corrected spectral density, Δ the distance, Q the quality factor, U the group velocity and v the seismograph magnification at a frequency f. The magnification v refers to that for the particle motion in the direction of the seismograph axis. We used $U = 4.35$ km/s and $Q = 110$ for Love waves, and $U = 3.9$ km/s and $Q = 130$ for Rayleigh waves. The quantity $|A_0(f)|$ can be regarded as the amplitude spectral density of the ground motion at $\Delta = 90°$ which would have been observed on a non-attenuating Earth, and was calculated for the stations listed in table 1 for comparison with the theoretical spectral density.

The theoretical spectral densities were calculated from SAITO's (1967) expression which was used by KANAMORI (1970a) for calculations of synthetic seismograms. For Love waves we started from eq. 1 of KANAMORI (1970a) and used the asymptotic expansion of spherical harmonics. After considerable algebraic operations, the transverse displacement $u_\phi(t)$ at a distance Δ and azimuth ϕ due to a point source varying stepwise in time can be written as

$$u_\phi(t) = 2 \int_0^{\infty} |G_\phi(f)| \cos[2\pi f t + \varepsilon_\phi(f)]\, df, \qquad (4)$$

TABLE 1(a)

Spectral densities of Love waves at a period of 100 s

Station	Distance (°)	Azimuth (°)	Component	$\lvert A_0(f)\rvert$ (cm · s)	$\lvert G_\phi(f)\rvert$ (cm · s)	M_0 (10^{28} dyne · cm)
Barcelona	92.7	333	E–W	55	1.30	4.2
Beograd	82.3	323	NW–SE	59	1.54	3.8
Helwan	87.3	307	E–W	91	1.60	5.7
Ksara	81.8	307	N–S	98	1.62	6.0
La Plata	161.7	104	N–S	26	0.80	3.3
Lund	76.8	334	NW–SE	49	1.26	3.9
Uppsala	72.0	335	E–W	51	1.26	4.0

TABLE 1(b)

Spectral densities of Rayleigh waves at a period of 100 s.
$|G(f)|$ represents $|G_r(f)|$ for the vertical component and $|G_\theta(f)|$ for the horizontal component

Station	Distance (°)	Azimuth (°)	Component	$\lvert A_0(f)\rvert$ (cm · s)	$\lvert G(f)\rvert$ (cm · s)	M_0 (10^{28} dyne · cm)
Barcelona	92.7	333	NE–SW	57	1.08	5.3
Copenhagen	77.0	334	U–D	34	1.16	2.9
Göttingen	81.2	333	U–D	60	1.20	5.0
Lund	76.8	334	NE–SW	25	0.80	3.1
Riverview	73.0	174	N–S	23	0.50	4.6
Strasbourg	84.5	333	U–D	43	1.20	3.6

where

$$|G_\phi(f)| = \frac{\pi a}{2U}(n+\tfrac{1}{2})(\tfrac{1}{2}\pi n \sin \Delta)^{-\frac{1}{2}}[(\Phi_{n,0}-\Phi_{n,2})^2+\Phi_{n,1}^2]^{\frac{1}{2}} \quad (5)$$

is the amplitude spectral density, and

$$\varepsilon_\phi(f) = -(n+\tfrac{1}{2})\Delta - \operatorname{arctg}\left[\frac{\Phi_{n,1}}{\Phi_{n,0}-\Phi_{n,2}}\right]+\tfrac{3}{4}\pi \quad (6)$$

is the phase delay. In these equations, a is the Earth's radius, U is the group velocity, n the order number of the free oscillation whose eigenfrequency is f, and

$$\Phi_{n,m} = (-n)^m \frac{y_{1,n}}{\sigma_n^2 I_{1,n}}(A_m^c \cos m\phi + A_m^s \sin m\phi), \quad (7)$$

where $y_{1,n}$ is the radial factor of the displacement of a normal mode of order n, σ_n is the angular eigenfrequency, $I_{1,n}$ is the energy integral, and A_m^c and A_m^s, which represent the geometry of the force, were defined in eq. 1 of KANAMORI (1970a).

Similarly, the spectral densities $|G_r(f)|$ and the phase delay $\varepsilon_r(f)$ of the vertical component of the Rayleigh wave displacement can be written as

$$|G_r(f)| = \frac{\pi a}{2U}(\tfrac{1}{2}\pi n \sin \Delta)^{-\frac{1}{2}}[(R_{n,0}-R_{n,2})^2+R_{n,1}^2]^{\frac{1}{2}} \quad (8)$$

and

$$\varepsilon_r(f) = -(n+\tfrac{1}{2})\Delta - \operatorname{arctg}\left[\frac{R_{n,1}}{R_{n,0}-R_{n,2}}\right]+\tfrac{1}{4}\pi, \quad (9)$$

where

$$R_{n,m} = (-n)^m \frac{y_{1,n}}{\sigma_n^2(I_{1,n}+N^2 I_{2,n})} \times (A_m^c \cos m\phi + A_m^s \sin m\phi), \quad (10)$$
$$N^2 = n(n+1).$$

The quantities $I_{1,n}$, $I_{2,n}$, A_m^c and A_m^s were given in eq. 2 of KANAMORI (1970a). The spectral density $|G_\theta(f)|$ and the phase delay $\varepsilon_\theta(f)$ of the radial component of the Rayleigh wave displacement can be written as

$$|G_\theta(f)| = (n+\tfrac{1}{2})\,|G_r(f)|\, y_{3,n}/y_{1,n}, \quad (11)$$

and

$$\varepsilon_\theta(f) = \varepsilon_r(f) - \tfrac{1}{2}\pi, \quad (12)$$

In eqs. (10) and (11), $y_{1,n}$ and $y_{3,n}$ are the radial factors of displacement of the spheroidal oscillation of order n.

Numerical calculations were made for the Earth model 5.08 M (PRESS, 1970; KANAMORI, 1970b) and for a focal depth of 16 km. The source was assumed to be a double-couple dip-slip fault with a dip direction of N 90° W and a dip angle of 45°. Spectral densities $|G(f)|$ at $\Delta = 90°$ and at azimuths corresponding to the stations listed in table 1 were calculated for a source moment of 10^{27} dyne · cm. The ratio $|A_0(f)|/|G(f)|$ gives the seismic moment in units of 10^{27} dyne · cm. The values of the moment thus determined (table 1) for stations at different azimuths and for Rayleigh and Love waves agree reasonably well with one another, indicating that the source geometry used here is reasonable. An average moment of $\overline{M}_0 = 4.3\times10^{28}$ dyne · cm is obtained. The average slip dislocation $\bar{u}$ on the fault plane is then obtained from

$$\bar{u} = M_0/\mu L w,$$

where μ is the rigidity, L the fault length and w the width of the fault plane. Assuming that the size of the aftershock area one day after the occurrence of the main shock represents the size of the fault plane, $L = 185$ km and $w = 100$ km can be obtained from fig. 6. With these values and $\mu = 0.7\times10^{12}$ dyne/cm^2,

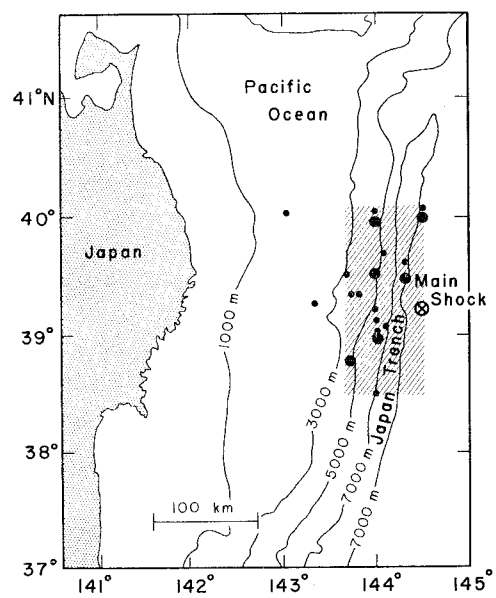

Fig. 6. Distribution of the aftershocks which occurred during the day following the main shock. The hatched area indicates the assumed fault plane. Large circles indicate larger aftershocks ($M \geqq 6.0$). The data are taken from the Catalogue of major earthquakes which occurred in and near Japan (1926–1956) (Japan Meteorological Agency, 1958).

$\bar{u}$ is estimated as 3.3 m. The location of the main shock with respect to the aftershock area (see fig. 6) suggests that the nodal plane dipping towards N 90° W is preferable for the fault plane. The dislocation of 3.3 m is in approximate agreement with that estimated from the amplitude of the tsunami. According to HONDA (1933), if the source area of the tsunami is assumed to be a circle with a diameter of D, the subsidence in the source area can be estimated as 2, 4 and 16 m for $D = 120$, 80 and 40 km, respectively. HATORI (1966) estimated, from energy considerations, that the vertical displacement in the source area is 7 to 8 m.

Although the fault dimensions estimated on the basis of the size of the aftershock area may be somewhat inaccurate, fault dimensions much smaller than those used above are by no means acceptable. The reason is that, for a given seismic moment, a smaller fault size requires a larger slip dislocation but too large a dislocation will be incompatible with the tsunami data. We therefore conclude that the Sanriku earthquake represents a normal faulting on a plane dipping 45° towards the continent and extending to a depth of $100 \times \cos 45° \approx 70$ km. Since the thickness of the lithosphere as estimated from the depth of the low-velocity zone is about 70 km (KANAMORI and PRESS, 1970), the above faulting involves the entire thickness of the lithosphere.

The stress drop associated with the faulting can be estimated, by using eq. 16 of AKI (1966), as 39 b. This value refers to the difference in stress before and after the formation of the fault, but not to the prevailing stress.

5. Near-field displacement

In the preceding analyses, we assumed that the first motion of the short-period (5 to 10 s) P waves represents the overall movement of the lithosphere. Some doubt, however, may be cast on the validity of this assumption; short-period waves may represent only the initial rupture of secondary importance, and not necessarily the major fracture of the lithosphere. Further, the surface wave amplitude may have been affected by the finiteness of the source and the lateral heterogeneity of the structure. In view of these considerations, an examination of our fault model on the basis of near-field observations is desirable.

At the time of the Sanriku earthquake, several classic long-period seismographs were operated at the University of Tokyo, about 500 km away from the epicenter. Fortunately, we found (in Prof. Matuzawa's collection) two horizontal seismograms, NS and EW components, for which the instrument constants were known. Figs. 7(a, b) show these seismograms; the pendulum periods are 33 and 50 s for EW and NS components, respectively. In order to examine whether our fault model is correct or not, synthetic seismograms were computed for our fault model and compared with the observed seismograms for both polarity and amplitude.

For the computation of the near-field displacement, we used HASKELL's (1969) compact formulations which give the displacement, in an infinite homogeneous medium, due to a propagating dislocation whose temporal variation is given by a ramp function. On account of the assumption of the infinite homogeneous medium, the comparison was inevitably limited to the initial portion of the seismogram, prior to the arrival of surface waves. The effect of the free surface was included simply by doubling the displacements calculated for an infinite medium. This procedure is probably acceptable at least for the initial half cycle of P and S waves.

We evaluated, by a numerical double integration, eqs. (4.1), (4.2) and (4.3) in HASKELL (1969) for the fault geometry determined by the first motions of P waves (45° normal dip–slip). Fig. 8 shows the fault geometry and the location of the station relative to the fault. The x_1 axis points towards the south and the x_2' axis towards the west. The station is located at the point P whose coordinates are $x_1 = 400$ km and $x_2' = 500$ km. The dislocation D_2 takes place simultaneously over the fault width w (= 100 km) in the x_2 direction, and propagates unilaterally at constant velocity v over a length L (= 185 km) in the positive x_1 direction. The sign of D_2 is taken such that the hanging-wall side displaces in the positive x_2 direction (normal fault). We assumed that the rise time of the ramp function was 10 s, the rupture velocity 3.5 km/s, the P velocity of the medium 8 km/s and the S velocity 4.6 km/s. A somewhat different choice of these rupture parameters would not significantly affect the wave form of such long-period waves as used here.

A detailed rupture process is not a matter of primary interest here; the direction of the motion and the

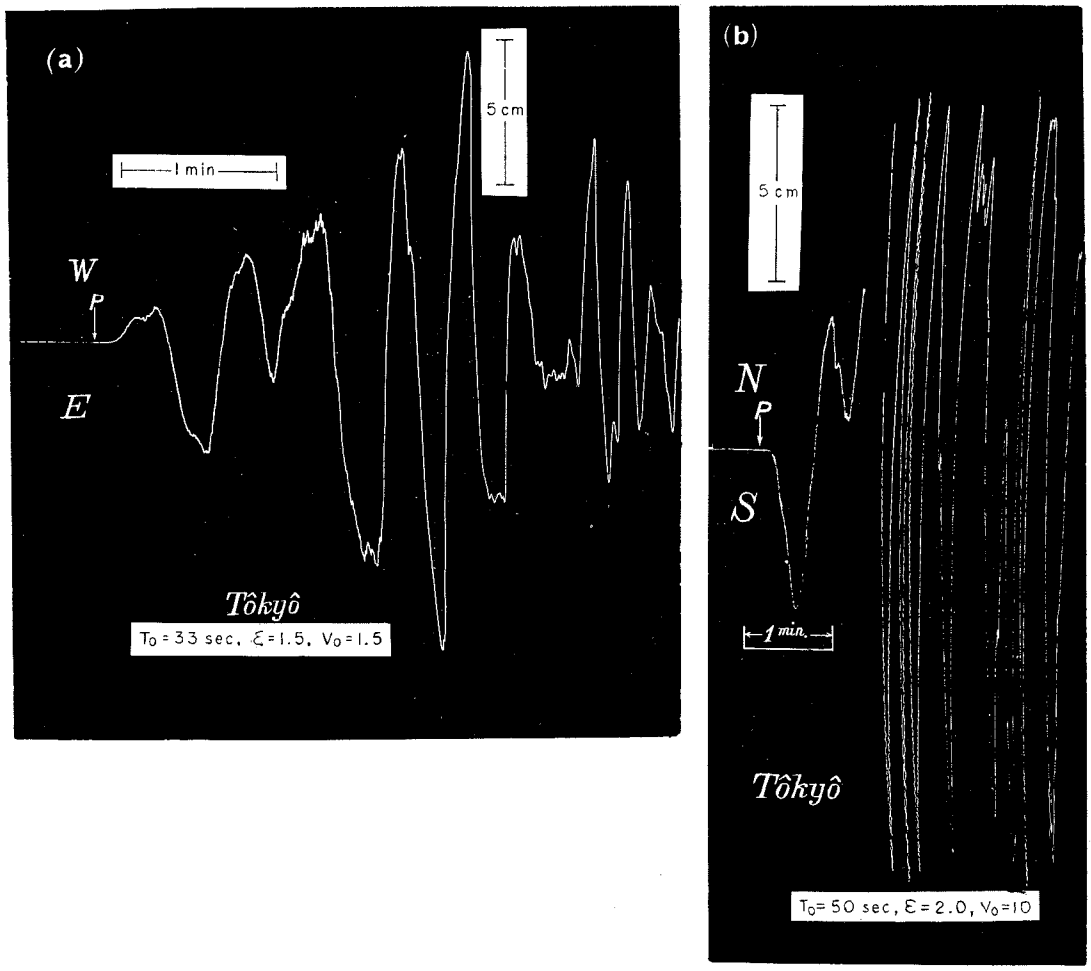

Fig. 7. Seismograms obtained by long-period horizontal seismographs installed at the University of Tokyo. (a) EW component; (b) NS component. T_0 is the pendulum period, ε the damping ratio and V_0 the magnification.

amplitude of at least the first half cycle of P and S waves are of primary importance. After the instrument response was included, the synthetic seismograms were computed for EW and NS components (see fig. 8) and compared with the observed seismograms as shown in figs. 9(a, b).

It is to be noted that the synthetic seismograms resemble the observed seismograms in two important respects: the direction of the first motion of P and S waves, and the amplitude of P waves relative to S waves. The discrepancy after the first half cycle of the P wave arrival is probably due to the effect of the free surface. By a direct comparison between the synthetic and observed seismograms for the amplitude of the initial half cycle of the P and S wave (only for the EW component), a dislocation D_2 of 5 m is obtained for the EW component and 2.5 m for the NS component (see figs. 9 and 10). This difference is partly due to the assumption of the homogeneity of the structure; the velocity gradient in the actual crust and mantle affects the angle of incidence, thereby changing the amplitude ratio of the NS to the EW component. An inaccurate instrument calibration may also be responsible for the difference. In any case, the dislocation of 2.5 to 5 m is in good agreement with that estimated from the surface wave amplitude.

Despite the gross simplification made in our calculation, the above result strongly supports our fault model. If we reduce the fault width to $\frac{1}{10}$, the dislocation required to explain the near-field displacement

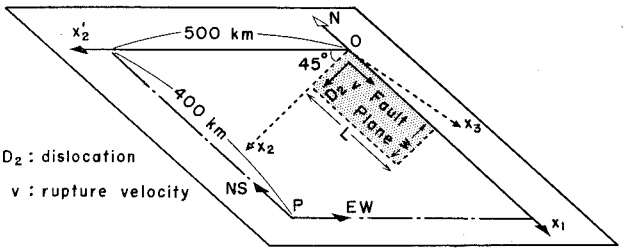

Fig. 8. Fault geometry used in the near-field calculation. D_2 – dislocation; w – fault width (= 100 km); v – rupture velocity.

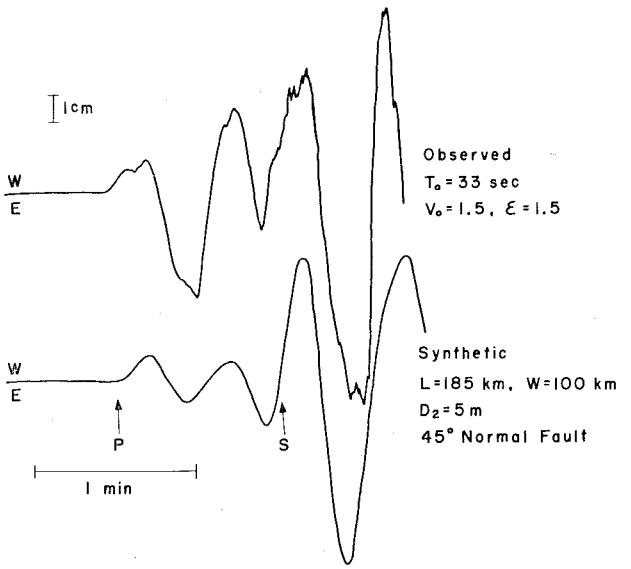

Fig. 9(a). Comparison of synthetic and observed (fig. 7a) seismograms, EW component. The synthetic seismogram is computed for a dislocation $D_2 = 5$ m. The times of P and S wave arrivals are indicated.

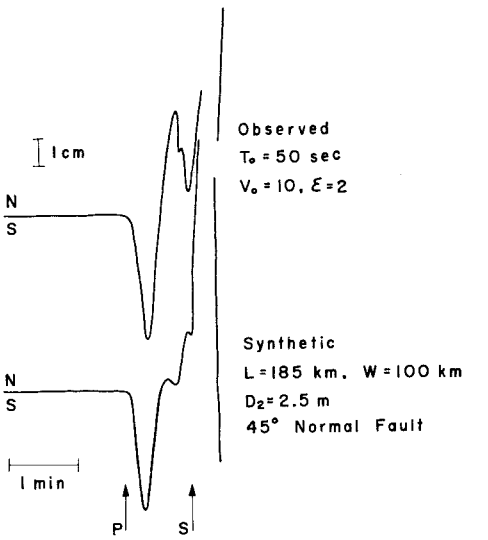

Fig. 9(b). Comparison of synthetic and observed (fig. 7b) seismograms, NS component. The synthetic seismogram is computed for a dislocation $D_2 = 2.5$ m. The times of P and S wave arrivals are indicated.

becomes about 25 to 50 m which is too large to be reconciled with the tsunami data (HONDA, 1933; HATORI, 1966). Thus the conclusion that the normal faulting associated with the Sanriku earthquake extends over nearly the entire thickness of the lithosphere is definitive.

6. Magnitude

RICHTER (1958) gave a magnitude of 8.9 to this earthquake. However, as pointed out by BRUNE and ENGEN (1969), the amplitude of the surface waves is not exceptionally large. The body wave, on the other hand, is very sharp (see fig. 3) and of large amplitude. This is not the case for other great earthquakes at island arcs. This unusual mode of radiation from the Sanriku earthquake is indicative of the special nature of the source, a slippage within a relatively homogeneous solid lithosphere.

Table 2 shows the surface wave (Rayleigh wave) magnitude M determined at several stations. The method is the same as that employed by KANAMORI and MIYAMURA (1970). The formula

$$M = \log(A/T) + 1.66 \log \Delta + 3.3$$

was used, where A is the amplitude in μm of the horizontal ground displacement which gives a maximum trace amplitude, T is the period in s, and Δ the distance in °. An average of 8.34 is obtained.

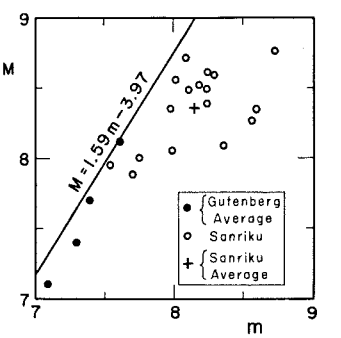

Fig. 10. Surface wave magnitude versus body wave magnitude.

Table 3 shows the body wave magnitude m determined on the basis of the charts given by GUTENBERG

and RICHTER (1956). The average value of m determined by the P waves is 8.16 (average period 9.4 s) and that by the S waves is 8.22 (average period 12.6 s). The average for both P and S waves is 8.18 (average period 10.5 s). This value of m leads to $M = 9.04$, through the formula $M = 1.59m - 3.97$ (GUTENBERG and RICHTER, 1956). Comparing this value with that obtained from the surface waves, we see that the Sanriku earthquake, as compared with other earthquakes, radiated a relatively large amount of energy in the form of short-period body waves. This situation is more clearly demonstrated in fig. 10 in which the values of M and m (for P waves) determined at the stations listed in tables 2 and 3 are plotted together with the average relation given by GUTENBERG (1956b) and with the straight line $M = 1.59m - 3.97$. None of the stations fall above the line. The radiation of short-period waves from the Sanriku earthquake is, on the average, $0.4m$ larger than that from "ordinary" earthquakes having a comparable magnitude in long-period radiation.

In general, the larger the ratio of the amplitude of short-period to long-period waves, the higher is the prevailing effective stress suggested at the earthquake source region (AKI, 1966; WYSS, 1970). However, a precise determination of the stress requires an accurate estimate of the wave energy which is carried mainly by short-period waves. Short-period waves, however, are substantially attenuated during the propagation and only a small fraction of their energy can be observed. We therefore did not estimate the stress, but the above result is probably sufficient for indicating that the Sanriku earthquake represents a faulting under a higher effective stress than "ordinary" earthquakes. Remembering the stress drop estimated in section 4, we conclude that the stress in the lithosphere changed, at a relatively high level, by 39 b at the time of the Sanriku earthquake.

7. Conclusion

Seismological evidence so far presented suggests, almost definitely, that the Sanriku earthquake of 1933 represents a release of a tensile stress on a fault plane extending over the entire thickness of the lithosphere; the average slippage on the fault plane, dipping 45° towards N 90° W, amounts to 3.3 m. This result precludes the possibility that the bending of the lithosphere is the principal cause of the Sanriku earth-

TABLE 2

Surface wave magnitude

Station	Distance (°)	Azimuth (°)	Amplitude (μm)	Period (s)	M
Adelaide	74.0	185	930	19	8.10
Barcelona	92.7	333	2750	20	8.71
Batavia	57.1	226	895	17	7.95
Beograd	82.3	323	2040	18	8.52
Berkeley	69.5	58	1040	20	8.08
Charlottsville	93.7	33	364	19	7.87
Copenhagen	77.0	334	3350	18	8.60
Göttingen	81.2	333	3100	25	8.56
Helwan	87.3	307	960	19	8.23
Karlsruhe	83.9	333	1980	20	8.49
Ksara	81.8	307	1600	20	8.38
La Plata	161.7	104	485	19	8.38
Leipzig	80.5	332	2090	20	8.48
München	83.4	331	2440	20	8.58
Rio de Janeiro	162.6	25	630	20	8.47
Riverview	73.0	174	850	19	8.04
Seattle	64.2	49	1680	19	8.26
Spokane	67.0	47	825	18	8.00
Strasbourg	84.5	333	3740	20	8.77
Ukiah	68.1	57	2030	20	8.35
Uppsala	72.0	335	1830	20	8.34
Wien	81.5	328	1220	17	8.33
Average					8.34 ± 0.25

TABLE 3

Body wave magnitude. A_{Pz} is the amplitude of the vertical component of P waves, A_{PH} the amplitude of combined horizontal component of P waves, and A_{SH} the amplitude of combined horizontal component of S waves. The average for P waves is 8.16 (average period 9.4 s) and the average for S waves 8.22 (average period 12.6 s)

Station	Distance (°)	Azimuth (°)	A_{Pz} (μm)	A_{PH} (μm)	A_{SH} (μm)	Period (s)	m
Barcelona	92.7	333	–	40	–	9	8.09
			–	–	170	14	8.03
Batavia	57.1	226	–	17	–	7	7.53
Beograd	82.3	323	–	110	–	11	8.19
			–	–	230	11	8.22
Berkeley	69.5	58	180	–	–	8	8.36
Charlottsville	93.7	33	–	14	–	8	7.70
Copenhagen	77.0	334	–	110	–	9	8.24
			–	–	390	14	8.34
Göttingen	81.2	333	–	66	–	10	8.01
Ivigtut	79.3	6	–	99	–	14	8.00
			–	–	230	15	7.96
Karlsruhe	83.9	333	–	80	–	8	8.24
			–	–	140	10	8.04
Ksara	81.8	307	–	120	–	11	8.25
			–	320	–	11	8.37
Leipzig	80.5	332	–	110	–	12	8.12
München	83.4	331	–	88	–	8	8.29
Paris	86.1	336	–	140	–	14	8.24
			–	–	420	16	8.21
Rivierview	73.0	174	–	56	–	9	8.00
Saint Louis	87.6	40	–	–	180	9	8.10
Seattle	64.2	49	–	130	–	7	8.57
			–	–	630	14	8.45
Spokane	67.0	47	–	42	–	7	7.75
			–	–	210	10	8.28
Strasbourg	84.5	333	–	150	–	5	8.72
			–	–	570	13	8.44
Ukiah	68.1	57	–	220	–	11	8.60
Uppsala	72.0	335	–	48	–	8	7.98
			–	–	330	13	8.30
Average						10.5	8.18

quake; the tensile stress caused by bending is significant only near the upper surface of the lithosphere. We prefer the interpretation that the Sanriku earthquake is a seismological manifestation of a large scale fracture of the lithosphere due to a gravitational pull exerted by the sinking lithosphere. This fracture probably took place on an old fault plane which had once fractured and healed up. The existence of this fracture zone accounts for the sharp bend of the lithosphere beneath the Japan trench. Thus, the sharp bend may be regarded as a result but not as the cause of great earthquakes beneath oceanic trenches. Further, the fracture zone decouples, to some extent, the lithosphere beneath the ocean basin from the sinking lithosphere; this idea is consistent with the abrupt disappearance of seismic activity at oceanic trenches in going from the continental to the oceanic side.

The Sanriku earthquake is probably the largest earthquake that represents a normal faulting and may as well be a relatively rare event. Nevertheless, it gives a crucial clue to the understanding of the mechanism of the bending and sinking of the lithosphere. It should be clearly recognized in discussions of island arc tectonics that this earthquake represents a tectonic phenomenon entirely different from that of other great earthquakes at island arcs; most of the great earthquakes at island arcs are characterized by more or less thrust faulting. The deformation of the lithosphere and the occurrence of great earthquakes at island arcs will be explained more fully, in conjunction with normal and thrust faultings, in a separate paper.

Acknowledgments

I am grateful to Professor Takeo Matuzawa who kindly provided me with valuable information concerning the seismograms he collected. I greatly benefited from discussions with K. Abe and Y. Fukao in various aspects of this study. I thank Professor S. Miyamura for the discussion on the body wave and surface wave magnitudes of this earthquake. Dr. K. Oike of Kyoto University kindly checked the numerical calculations of near-field displacements. Dr. Tomowo Hirasawa generously allowed me to use his computer program for the focal mechanism determination from S wave data.

References

AKI, K. (1966), Bull. Earthquake Res. Inst. Tokyo Univ. **44,** 73–88.

BRUNE, J. N. and G. R. ENGEN (1969), Bull. Seismol. Soc. Am. **59,** 923–933.

BRUNE, J. N. and C. Y. KING (1967), Bull. Seismol. Soc. Am. **57,** 1355–1365.

GUTENBERG, B. (1956a), Trans. Am. Geophys. Union **37,** 608–614.

GUTENBERG, B. (1956b), Bull. Seismol. Soc. Am. **46,** 105–145.

GUTENBERG, B. and C. F. RICHTER (1954), *Seismicity of the Earth and associated phenomena*, 2nd ed. (Princeton Univ. Press, Princeton) 135.

GUTENBERG, B. and C. F. RICHTER (1956), Ann. Geofis. Rome **9,** 1–15.

HASKELL, N. A. (1969), Bull. Seismol. Soc. Am. **59,** 865–908.

HATORI, T. (1966), Bull. Earthquake Res. Inst. Tokyo Univ. **44,** 1449–1464.

HIRASAWA, T. (1966), Bull. Earthquake Res. Inst. Tokyo Univ. **44,** 901–918.

HONDA, H. (1933), Kenshin Jiho **7,** 155–159 (in Japanese).

Japan Meteorological Agency, Catalogue of major earthquakes which occurred in and near Japan (1926–1956), in *The Seismological Bulletin of the Japan Meteorological Agency, Supplementary Volume No. 1*, pp. 1–91, Tokyo, 1958.

KANAMORI, H. (1970a), J. Geophys. Res. **75,** 5011–5027.

KANAMORI, H. (1970b), Phys. Earth Planet. Interiors **2,** 259–275.

KANAMORI, H. and F. Press (1970), Nature **226,** 330–331.

KANAMORI, H. and S. MIYAMURA (1970), Bull. Earthquake Res. Inst. Tokyo Univ. **48,** 115–125.

MATUZAWA, T. (1935), Bull. Earthquake Res. Inst. Tokyo Univ. **13,** 171–193.

MATUZAWA, T. (1942), Bull. Earthquake Res. Inst. Tokyo Univ. **20,** 162–171.

PRESS, F. (1970), Phys. Earth Planet. Interiors **3,** 3–22.

RICHTER, C. F. (1958), *Elementary seismology* (Freeman, San Francisco, Calif.) 712.

SAITO, M. (1967), J. Geophys. Res. **72,** 3689–3699.

STAUDER, W. (1968a), J. Geophys. Res. **73,** 3847–3858.

STAUDER, W. (1968b), J. Geophys. Res. **73,** 7693–7701.

WYSS, M. (1970), J. Geophys. Res. **8,** 1529–1544.